





# Dynamically Scaled Temperature in Self-Supervised Contrastive Learning

Siladitya Manna<sup>1</sup>, Soumitri Chattopadhyay<sup>2</sup>, Rakesh Dey<sup>1</sup>, Saumik Bhattacharya<sup>3</sup>, and Umapada Pal<sup>1</sup>

<sup>1</sup> Indian Statistical Institute, Kolkata

<sup>2</sup> UNC Chapel Hill

<sup>3</sup> Indian Institute of Technology Kharagpur

**Abstract.** In contemporary self-supervised contrastive algorithms like SimCLR, MoCo, etc., the task of balancing attraction between two semantically similar samples and repulsion between two samples of different classes is primarily affected by the presence of hard negative samples. While the InfoNCE loss has been shown to impose penalties based on hardness, the temperature hyper-parameter is the key to regulating the penalties and the trade-off between uniformity and tolerance. In this work, we focus our attention on improving the performance of InfoNCE loss in self-supervised learning by proposing a novel cosine similarity dependent temperature scaling function to effectively optimize the distribution of the samples in the feature space. We also provide mathematical analyses to support the construction of such a dynamically scaled temperature function. Experimental evidence shows that the proposed framework outperforms the contrastive loss-based SSL algorithms. Our code is available at <https://www.github.com/subanon/dystress>.

**Keywords:** Self-supervised · Contrastive · Temperature

## 1 Introduction

With its prowess at learning high-quality representations from large-scale unlabeled data, self-supervised learning (SSL) has revolutionized the field of machine learning. Classical approaches in SSL involved designing a suitable pretext task, such as solving jigsaw puzzles [33], image inpainting [35], colorization [50], etc. However, the problem with these methods was that there exists a significant difference between the nature of the pretext task and the desired downstream task (classification/segmentation). Recent works have focused on contrastive learning framework [6, 19, 47], wherein the model learns an embedding space such that the features of augmented versions of the same sample lie close to each other, pushing the embeddings of other samples farther apart. Thus, unsupervised contrastive models, aided by heavy augmentations and robust abstractions, are capable of learning certain levels of representational structures. Empirically, contrastive learning-based algorithms have been found to perform better at downstream tasks than the former SSL methods.

The most commonly used loss function for self-supervised contrastive learning (SSCL) is the InfoNCE loss, used in several works such as CPC [34], MoCo [19], SimCLR [6], etc. Although the temperature hyper-parameter is an integral part of the InfoNCE function, it has mostly been trivialized as a mere scaling coefficient. Recently, in [28] the authors have proposed a temperature hyper-parameter ( $\tau$ ) scheduling for SSL. However, the method proposed in [28] is mainly focused on task switching based on the temperature hyper-parameter  $\tau$  rather than focusing on the effect of  $\tau$  on false negative samples. In our work, however, we argue that there is more to this seemingly redundant factor. Our theoretical analyses bring forth an intuitive yet vital aspect related to the presence of constructively false negative yet inherently positive pairs – samples that do not originate from the same instance yet show a high degree of semantic representational similarity as they belong to the same underlying class. As the main objective of the contrastive loss function is to maximize the similarity of the different augmentations of the same instance while minimizing the same for different instances, the aforementioned constructively false negative pairs are repelled away. This action implies that semantic information is not an integral part of existing InfoNCE loss. Pushing the samples in semantically similar pairs away creates an adverse effect on representation learning. Large penalties on these samples along with true negative samples may increase the uniformity, but it adversely affects the alignment of the local structure constituted by samples with similar semantic information. Hence the uniformity-tolerance (alignment) dilemma arises as addressed in [43]. In this work, we intend to dynamically scale the temperature hyper-parameter as a function of the cosine similarity to effectively control the repelling effect in these false negative pairs. We theorize that scaling the temperature dynamically will prevent disruption of the local and global structures of the feature space and improve representation learning.

The primary contributions of the proposed method called DySTreSS can be summarized as follows:

- We systematically study the role of temperature hyper-parameter and its effect on local and global structures in the feature space during optimization of the InfoNCE loss, both intuitively and theoretically, to establish the motivation for our proposed method. To the best of our knowledge, this is the first exhaustive attempt to design a temperature function that can be adaptively tuned based on local and global structures.
- With the established groundwork, we propose a temperature-scaled contrastive learning framework (DySTreSS) that dynamically modulates the temperature hyperparameter.
- We show the effectiveness of our approach by conducting experimentation across several benchmark vision datasets, with empirical results showing that our method outperforms better than several state-of-the-art SSL algorithms in the literature.

The rest of the paper is organized as follows. Sec. 2 briefs contemporary works in self-supervised learning, along with an account of the works where the

temperature hyper-parameter is the focus point. Sec. 3.1 gives a detailed account of the theoretical background. Sec. 3 discusses the motivation and also introduces the proposed framework. Next, we present the implementation details in Sec. 4. The experimental evidence, along with various ablation studies, are presented with illustrations in Sec. 5. Finally, we conclude our work in Sec. 6.

## 2 Related Work

**Self-supervised Learning.** SSL approaches [1, 6–9, 16, 24, 47, 48] have become the de facto standard in unsupervised representation learning with the aim to learn powerful features from unlabelled data that can be effectively transferred to downstream tasks. Several pre-training strategies have been proposed, which can be categorized as generative or reconstruction-based [15, 26, 29, 36, 50], clustering-based [2–4, 22], and contrastive learning approaches [6–8, 19, 47]. Other popular methods include similarity learning [9], redundancy reduction within embeddings [48], and an information maximization-based algorithm [1]. Recently, self-distillation based frameworks like [5], [53], etc. have also shown significant improvement in performance.

**Contrastive Learning.** The majority of recent SSL algorithms have leveraged contrastive learning, which causes distorted versions of the same sample to attract and different samples to repel. SimCLR [6] simply used a contrastive loss function with a large batch size, while MoCo [19] leveraged momentum encoding and a dictionary-based feature bank for negative samples. These works were further enhanced in [7] and [8] respectively. Recent works like DCL [47] where the authors decoupled the positive and negative pairing components of the InfoNCE [18] loss function.

Recently, negative-free contrastive learning frameworks like ZeroCL [52], WMSE [12], ARB [51] have also gained much attention. However, ZeroCL and WMSE use negative samples for calculating dimension-wise statistics. Hence, in a way, they depend on the negative samples. WMSE also involves a Cholesky decomposition step, which has a high computational complexity. The most recent work ARB improves upon the Barlow Twins method, by using the nearest orthonormal basis-based optimization objective. However, it uses a spectral decomposition step to deal with non-full rank matrices, which can be quite computationally expensive.

**Temperature in Contrastive Learning.** Recently, there have been a few pieces of work that have focused on the temperature hyper-parameter in the InfoNCE loss function. In [49], the authors present a temperature hyper-parameter as a function of the input representations thereby incorporating uncertainty in the form of temperature. [43] explores the hardness-aware property of contrastive loss and the role of temperature in it by measuring the uniformity and tolerance of representations. On the other hand, MACL [55] assumed the temperature hyperparameter as the function of alignment to address the uniformity-tolerance dilemma that exists in the InfoNCE loss design. Motivated by the study shown in [43], the authors in [28] proposed a continuous task switching between instance

discrimination and group-wise discrimination by using simple cosine scheduling. In [37], the authors attempt to implement distributionally robust optimization for individual temperature individualization, that is, it uses a temperature hyper-parameter  $\tau_i$  corresponding to each anchor sample  $x_i$ , and is updated at each iteration. This no longer keeps the temperature as a hyper-parameter and converts it into another optimizable parameter.

### 3 Methodology

#### 3.1 Theoretical Background

In self-supervised contrastive learning [6, 19, 34], the InfoNCE loss is given by Eqn. 1.

$$\mathcal{L} = \sum_i \mathcal{L}_i = - \sum_i \ln(p_{ii+}) = - \sum_i \ln \left( \frac{\exp(\frac{s_{ii+}}{\tau})}{\sum_j \exp(\frac{s_{ij}}{\tau})} \right) \quad (1)$$

where  $ii+$  denotes a true positive pair and  $s_{ij}$  is the cosine similarity between the latent vectors of the samples  $x_i$  and  $x_j$ . In self-supervised contrastive learning frameworks like SimCLR [6], MoCo [19], etc., we assume that each sample is a class on its own. This results in the pairing of any two samples that may belong to the same class, resulting in the formation of false negative (FN) pairs. The similarity between these samples in these types of pairs can assume high cosine similarity values. On the contrary, pairs consisting of two samples belonging to two different classes comprise true negative (TN) pairs. However, depending on the mapping of the corresponding features to the feature space, true negative pairs can also have high cosine similarity between the constituent samples, and are called hard true negative pairs. False negative pairs by construction can also act as hard false negative pairs. True positive (TP) pairs are simply constituted of samples obtained by two random augmentations of a sample in the dataset.

#### 3.2 Role of Temperature in Contrastive Learning

InfoNCE loss concentrates on optimization by penalizing the hard negative pairs according to their hardness [43]. The gradient of  $\mathcal{L}_i$  w.r.t.  $s_{ii}$  and  $s_{ij}$  is given by Eqn. 2 and 3. A simple relative weightage is defined in [43] and as given in Eqn. 4.

$$\frac{\partial \mathcal{L}_i}{\partial s_{ii+}} = -\frac{1}{\tau} \sum_{k \neq i} p_{ik} \quad (2) \quad \frac{\partial \mathcal{L}_i}{\partial s_{ij}} = \frac{1}{\tau} p_{ij} \quad (3) \quad r(s_{ij}) = \frac{|\frac{\partial \mathcal{L}_i}{\partial s_{ij}}|}{|\frac{\partial \mathcal{L}_i}{\partial s_{ii+}}|} = \frac{\exp(\frac{s_{ij}}{\tau})}{\sum_{k \neq i} \exp(\frac{s_{ik}}{\tau})} \quad (4)$$

Therefore, the role of temperature  $\tau$  in contrastive loss is to control the relative weightage of the hard negative samples. As a result, low temperature values tend to penalize more without semantic similarity awareness and create a more uniformly distributed feature space. Hence, it is evident that the temperature hyper-parameter acts as the control knob for the uniformity.

### 3.3 Effect of Temperature on Local and Global Structures

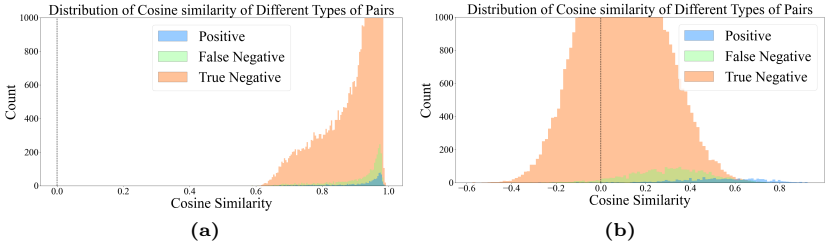


**Fig. 1:** (a) Histogram of cosine similarities of true positive (TP), false negative (FN), and true negative (TN) pairs at random initialization, (b) Histogram of cosine similarities of TP, FN, and TN pairs after pre-training. (Best viewed at 300%)

Let us assume that for a given sample  $x$ , we have an encoder  $f : x \rightarrow z \in \mathbb{R}^D$ , where  $z$  is a mapped image. Under any valid distance measure  $\mathfrak{M}$  on the manifold  $\mathfrak{U}$  of  $z$ , in an optimal scenario, if convergence is achieved in a self-supervised pre-training stage, two mapped images  $z_i$  and  $z_j$ , where  $i \neq j$ , from same class  $C$ , will have minimum possible distance. In our work, the term ‘local structure’ of any sample refers to the arrangement of the other samples in the close local neighborhood of that sample and can be denoted by the samples included in a closed ball of radius  $r_j$  around centroid sample  $x_j$ . Likewise, the term ‘global structure’ takes the arrangement of all the samples in the feature space into account.

As already stated in Sec. 3.2, decreasing the temperature tends to penalize the hard negative pairs more. This is because hard negative pairs tend to have high cosine similarity (say,  $s_{ij}$ ). With small temperature, the quantity  $\frac{s_{ij}}{\tau}$  is further amplified, consequently resulting in a larger penalty (from Eqn. 4). This causes samples constituting false negative pairs to drift apart. Consequently, the local structure consisting of samples of any particular class is disturbed. This effect on false negative pairs gives rise to the “uniformity-tolerance dilemma”.

The effect of temperature can be better understood if we take the gradient of the loss with respect to any latent vector  $z_j$ . Taking the expression of the derivative of the loss  $\mathcal{L}$ , given by Eqn. 1, with respect to  $z_j$ , we get

$$\begin{aligned} \frac{\partial \mathcal{L}}{\partial z_i} &= \left[ -\frac{z_{i^+}}{\tau} + \frac{\frac{z_{i^+}}{\tau} \cdot e^{C_{ii^+}} + \sum_{\substack{j=1 \\ j \neq i}}^N \frac{z_j}{\tau} \cdot e^{C_{ij}}}{e^{C_{ii^+}} + \sum_{\substack{j=1 \\ j \neq i}}^N e^{C_{ij}}} \right] + \sum_{\substack{j=1 \\ j \neq i}}^N \frac{\frac{z_j}{\tau} \cdot e^{C_{ji}}}{e^{C_{jj^+}} + \sum_{\substack{k=1 \\ k \neq j}}^N e^{C_{jk}}} \\ &= - \left[ \frac{z_{i^+}}{\tau} (1 - p^{ii^+}) - \sum_{\substack{j=1 \\ j \neq i}}^N \frac{z_j}{\tau} (p^{ij} + p^{ji}) \right] \end{aligned} \quad (5)$$

where  $C_{ij} = \frac{s_{ij}}{\tau}$ , denotes the cosine similarity between the feature vectors  $z_i$  and  $z_j$ , scaled by temperature  $\tau$ , and  $(z_i, z_{i+})$  forms the positive pair. The quantity  $p^{i\psi j}$  is the probability of the pair  $(x_i, x_j)$  being predicted as a positive pair with the sample  $x_i$  as the anchor. Hence, from the expression of the displacement vector  $\frac{\partial \mathcal{L}}{\partial z_i}$ , we can arrive at the conclusion that at a low-temperature value the sample  $z_i$  moves away from any sample  $z_j$  if they are mapped close to each other in the feature space. In other words, contrastive loss penalizes hard negative pairs. The effect of temperature reduction in different scenarios is discussed as follows.

**Reducing Temperature for False Negatives:** By Gradient Descent rule,  $z_i^{t+1} = z_i^t - \frac{\partial \mathcal{L}}{\partial z_i}$ . The contribution of false negative pairs should be negative to the gradient of  $\mathcal{L}$  with respect to the feature (latent) vector  $z_i$ . For false negative pairs, the value of cosine similarity between the two elements in the pair can be positive or negative depending on where the samples are mapped. Adjusting the temperature hyper-parameter allows us to control the contribution of the false negative pairs in the loss optimization process, by scaling the weights of the latent vectors. For two closely placed false negative samples, the sum of the corresponding probabilities  $p^{i\psi j} + p^{j\psi i}$  as shown in Eqn. 5 will be high. If the temperature is decreased, the contribution of the sample  $z_j$  in the gradient increases further, resulting in the sample  $z_i$  drifting opposite to the direction of  $z_j$ . Conversely, if we take the derivative of  $\mathcal{L}$  with respect to  $z_j$  similar to Eq. 5, we will get a term involving  $z_i$ , which will enforce a similar effect on  $z_j$ . This results in the disruption of the local cluster structure in the feature space.

**Reducing Temperature for Hard Negatives:** For hard negative pairs, we can expect the two constituent samples to drift apart from each other if a low enough temperature is applied. However, without a ground truth label, it is impossible to apply selective temperature moderation to all the pairs. If we decrease the temperature for all pairs whose cosine similarity is above a certain threshold (say,  $C_\alpha$ ), then the closely spaced false negative pairs will also be affected, resulting again in disruption of the local cluster structure.

**What if there were no False Negatives?** In an ideal scenario, where all the negative pairs are true negative pairs (like in supervised contrastive learning [25]), we may make the mistake of assuming that we can safely decrease the temperature. Decreasing the temperature for true negative pairs will certainly improve performance up to a certain level, below which the performance degrades due to numerical instability [25], as the gradients become too large. This degradation in performance is due to the disruption in the global structure of the feature space. Disruption in local structure causes degradation of alignment in the feature space, whereas disruption in the global structure will cause an increase in uniformity [43, 45].

**Increasing Global Temperature:** On the other hand, increasing the temperature for all the samples has the opposite effect. As the temperature is increased, the drift in the false negative pairs is reduced, thereby helping in maintaining proper alignment. However, the uniformity may be affected as the repulsion between samples constituting true negative pairs including the hard

true negatives, will also be reduced. Hence, increasing temperature causes an increase in alignment but affects uniformity.

### 3.4 Motivation of Proposed Temperature Scaling Function

In SSCL, we can neither know for certain the boundary between true and false negatives, nor the class labels. However, we have described the effect of temperature on the feature space in the Sec. 3.3 and can list some criteria we need to follow to design a proper temperature scaling function. The criteria are as follows: (1) *Local criteria*: A very low temperature in both the highly positive and negative cosine similarity region will disrupt the local structure, (2) *False negative criteria*: A very low temperature for false negative pairs, which we can assume to lie in the range  $[s_{fn}, +1.0]$  can affect hard true negative and true positive pairs, where  $s_{fn}$  denotes a cosine similarity score, (3) *Global criteria*: A high temperature will affect the uniformity of the feature space and delay convergence.

Let us assume  $\tau(\cdot)$  is the temperature function, which takes the cosine similarity of a pair as input and outputs a temperature value for the same. For the rest of this literature, we will consider  $\tau_{ij} = \tau(s_{ij})$ .

$$\frac{\partial \mathcal{L}_i}{\partial s_{ii+}} = -\frac{\tau_{ii} - s_{ii+} \frac{\partial \tau_{ii}}{\partial s_{ii+}}}{\tau_{ii}^2} \cdot (1 - p_{ii+}) \quad (6) \quad \frac{\partial \mathcal{L}_i}{\partial s_{ij}} = \frac{\tau_{ij} - s_{ij} \frac{\partial \tau_{ij}}{\partial s_{ij}}}{\tau_{ij}^2} \cdot p_{ij} \quad (7)$$

where  $s_{ii+}$  and  $s_{ij}$  denote the cosine similarity of positive and negative pairs, respectively.

For negative pairs,  $\frac{\partial \mathcal{L}}{\partial s_{ij}} = \delta > 0$ , where  $\delta$  is a non-negative number. From Eqn. 7, we get,

$$\frac{\partial \mathcal{L}}{\partial s_{ij}} = \frac{\tau_{ij} - s_{ij} \frac{\partial \tau_{ij}}{\partial s_{ij}}}{\tau_{ij}^2} p_{ij} = \delta \quad \text{where } \delta < \epsilon \text{ and } \delta, \epsilon > 0 \quad (8)$$

Now, we will try to build a few assumptions about our proposed temperature function, and later we will show that these assumptions hold true by solving a differential equation arising from Eqn. 6 and 7. It is to be noted, that the following assumptions about the slope of the temperature function do not influence the derivation in any way. Without loss of generality, we can always assume  $\tau_{ij} > 0$ . As the temperature parameter cannot be negative, the temperature value would be 0.0 or some positive constant. For  $s_{ij} < 0$ , to satisfy our criteria (1) and (2), we should have  $\frac{\partial \tau_{ij}}{\partial s_{ij}}$  always less than some negative number. Hence, the slope of the temperature function is negative in the negative half of the cosine similarity vs. temperature plane. In the positive half of the cosine similarity vs. temperature plane, the slope of the temperature function is less than some positive number. However, a negative slope in the positive half would mean that temperature would decrease at high cosine similarity, again violating our criteria (1) and (2). A low temperature at high cosine similarity will affect the hard negative pairs and degrade the local structure. Taking into consideration the above two assumptions,

we should adopt the temperature function such that the temperature does not violate criteria (3) at high cosine similarity values.

**Proposition 1:** *The temperature function should have a negative and positive slope in the negative and positive half of the cosine similarity vs. temperature plane, respectively.*

**Proof:**

For negative pairs, the gradient of the InfoNCE loss with respect to  $s_{ij}$  will be non-negative, because, if loss decreases, then the cosine similarity of negative pairs should decrease. We assume that the value of this gradient is  $\delta$ , as shown in Eqn. 9.

$$\frac{\partial \mathcal{L}}{\partial s_{ij}} = \frac{\tau_{ij} - s_{ij} \frac{\partial \tau_{ij}}{\partial s_{ij}}}{\tau_{ij}^2} p_{ij} = \delta \text{ where } \delta < \epsilon \text{ and } \delta, \epsilon > 0 \quad (9)$$

where  $\epsilon$  is a small non-negative number. Expanding the Eqn. 9, we get,

$$\begin{aligned} \frac{\tau_{ij} - s_{ij} \frac{\partial \tau_{ij}}{\partial s_{ij}}}{\tau_{ij}^2} p_{ij} &= \delta \\ \implies \frac{\tau_{ij} - s_{ij} \frac{\partial \tau_{ij}}{\partial s_{ij}}}{\tau_{ij}^2} &= \frac{\delta}{p_{ij}} \\ \implies \tau_{ij} - s_{ij} \frac{\partial \tau_{ij}}{\partial s_{ij}} &= \tau_{ij}^2 \frac{\delta}{p_{ij}} \\ \implies \frac{\partial \tau_{ij}}{\partial s_{ij}} &= \frac{1}{s_{ij}} \left[ \tau_{ij} - \tau_{ij}^2 \frac{\delta}{p_{ij}} \right] \\ \implies \frac{\partial \tau_{ij}}{\partial s_{ij}} &= \frac{\tau_{ij}}{s_{ij}} \left[ 1 - \frac{\tau_{ij} \delta}{p_{ij}} \right] \end{aligned} \quad (10)$$

We can assume that  $\tau_{ij} > 0$  without loss of generality.

In self-supervised contrastive learning, the temperature should be high for false negatives to prevent too much repulsion. We have discussed the criteria and the motivation behind our temperature function in Sec. 3.4 of the main manuscript. Also, the temperature should not be very small in the regions with highly negative cosine similarity. We assume that the number of false negatives decreases as we move towards the point  $s_{ij} = 0.0$ . Hence, for the vanilla case, we will consider two regions, (1)  $s_{ij} > 0$  and (2)  $s_{ij} \leq 0$ .

Expanding the expression for  $p_{ij}$  in Eqn. 10, we get,



$$\begin{aligned}
 \frac{\partial \tau_{ij}}{\partial s_{ij}} &= \frac{\tau_{ij}}{s_{ij}} \left[ 1 - \frac{\tau_{ij} \delta}{\frac{\exp(s_{ij}/\tau_{ij})}{\sum_{k=1}^N \exp(s_{ik}/\tau_{ik})}} \right] \\
 \Rightarrow \frac{\partial \tau_{ij}}{\partial s_{ij}} &= \frac{\tau_{ij}}{s_{ij}} \left[ 1 - \frac{\tau_{ij} \delta \sum_{k=1}^N \exp(s_{ik}/\tau_{ik})}{\exp(s_{ij}/\tau_{ij})} \right] \\
 \Rightarrow \frac{\partial \tau_{ij}}{\partial s_{ij}} &= \frac{\tau_{ij}}{s_{ij}} \left[ 1 - \tau_{ij} \delta \frac{\exp(s_{ij}/\tau_{ij}) + \sum_{\substack{k=1 \\ k \neq j}}^N \exp(s_{ik}/\tau_{ik})}{\exp(s_{ij}/\tau_{ij})} \right] \\
 \Rightarrow \frac{\partial \tau_{ij}}{\partial s_{ij}} &= \frac{\tau_{ij}}{s_{ij}} \left[ 1 - \tau_{ij} \delta \frac{\exp(s_{ij}/\tau_{ij}) + \sum_{\substack{k=1 \\ k \neq j}}^N \exp(s_{ik}/\tau_{ik})}{\exp(s_{ij}/\tau_{ij})} \right] \\
 \Rightarrow \frac{\partial \tau_{ij}}{\partial s_{ij}} &= \frac{\tau_{ij}}{s_{ij}} \left[ 1 - \tau_{ij} \delta \left( 1 + \frac{\sum_{\substack{k=1 \\ k \neq j}}^N \exp(s_{ik}/\tau_{ik})}{\exp(s_{ij}/\tau_{ij})} \right) \right] \\
 \Rightarrow \frac{\partial \tau_{ij}}{\partial s_{ij}} &= \frac{\tau_{ij}}{s_{ij}} \left[ 1 - \tau_{ij} \delta \left( 1 + K \cdot \exp\left(-\frac{s_{ij}}{\tau_{ij}}\right) \right) \right]
 \end{aligned} \tag{11}$$

where  $K = \sum_{\substack{k=1 \\ k \neq j}} \exp\left(\frac{s_{ik}}{\tau_{ik}}\right)$  is taken as a constant with respect to  $s_{ij}$ , that is,

$$\frac{\partial K}{\partial s_{ij}} = 0.$$

If  $N \rightarrow \infty$  or for very large  $N$ , we can safely assume

$$\frac{\exp(s_{ij}/\tau_{ij}) + \sum_{\substack{k=1 \\ k \neq j}}^N \exp(s_{ik}/\tau_{ik})}{\exp(s_{ij}/\tau_{ij})} \simeq \frac{\sum_{\substack{k=1 \\ k \neq j}}^N \exp(s_{ik}/\tau_{ik})}{\exp(s_{ij}/\tau_{ij})} = K \cdot \exp\left(-\frac{s_{ij}}{\tau_{ij}}\right) \tag{12}$$

Hence, Eqn. 11 reduces to,

$$\frac{\partial \tau_{ij}}{\partial s_{ij}} = \frac{\tau_{ij}}{s_{ij}} \left[ 1 - \tau_{ij} \delta \left( K \cdot \exp\left(-\frac{s_{ij}}{\tau_{ij}}\right) \right) \right] \tag{13}$$

Solving the first-order nonlinear ordinary differential equation given by Eqn. 13, we get,

$$\tau_{ij} = \frac{s_{ij}}{\log(\delta \cdot K \cdot s_{ij} - c)} \tag{14}$$

where  $c$  is the integral constant.

To find the value of  $c$ , we have to solve for the value of  $\tau_{ij}$  at the endpoints of the cosine similarity line. It is to be remembered,  $\tau_{ij}$  takes the value  $\tau_{max}$  at  $s_{ij} = -1$  and  $s_{ij} = +1$  (Please refer to Sec. 3.4 in the main manuscript).

Solving, the above equation for the two above-mentioned cases, we get,

$$\begin{aligned}
 c^- &= -\delta \cdot K - \exp(-1/\tau_{max}) \\
 c^+ &= -\delta \cdot K - \exp(1/\tau_{max})
 \end{aligned} \tag{15}$$

Varying the value of the constant in the range  $[c^-, c^+]$ , we get different curves with different slopes for different values of  $\delta$  and  $K$ , as shown in the Fig. 2

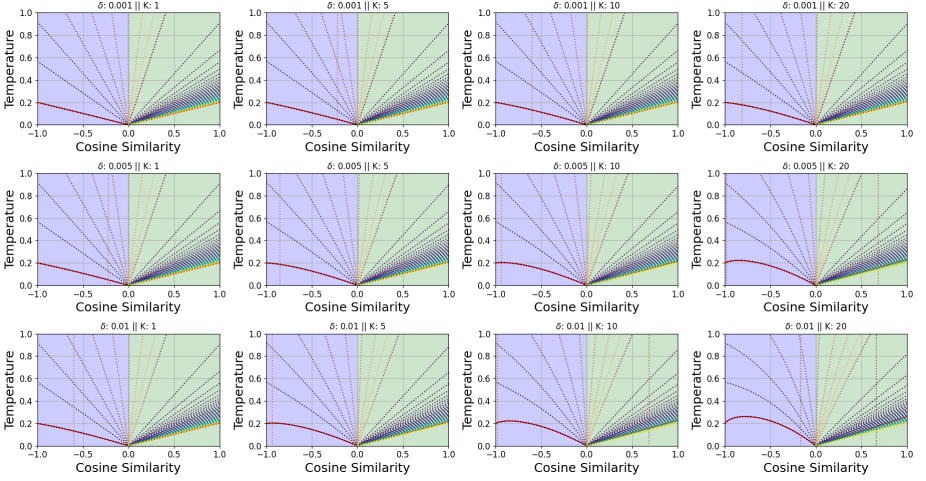


**Fig. 2:** Plots of the solution of ODE in Eqn. 14 for different values of the integral constant, over different values of  $\delta$  and  $K$ .

We can observe, that the plotted curves in Fig. 2 do in fact show positive and negative gradients on the positive and negative half of the cosine similarity vs. temperature plane, respectively, as stated in the Sec. 3.4 of the main manuscript. This establishes our theoretically derived condition for the slopes of the temperature function.

As shown in Fig. 2, we can observe that the plotted curves show positive and negative gradients on the positive and negative half of the cosine similarity vs. temperature plane, respectively, as stated in this section. This establishes our intuitively derived assumptions for the slopes of the temperature function in the negative and positive halves of the cosine similarity vs. temperature plane. The detailed proof of the proposition is given in Appendix ??.

### 3.5 Proposed Framework

Combining all the above philosophies together we describe the framework proposed in this work. In this work, we use SimCLR [6] as the baseline framework. To satisfy the conditions derived in the section above, we adopt a cosine function of the cosine similarity as the temperature function, as shown in Alg. 1. We can visualize from Fig. 3, that the cosine function does not violate the four criteria mentioned in Sec. 3.4.

---

**Algorithm 1:** Temperature Scaling Function
 

---

**Data:**  $\tau_{max}$  and  $\tau_{min}$

**Input:**  $s_{ij} \rightarrow$  Cosine Similarity of the pair  $(x_i, x_j)$

$$\tau_{ij} = \tau_{min} + 0.5 \times (\tau_{max} - \tau_{min}) \times (1 + \cos(\pi(1 + s_{ij})))$$


---

For different  $\tau_{max}$  and  $\tau_{min}$  values, we obtain different temperature scaling functions as shown in Fig. 3. In Table 10, we also show the comparison of different temperature functions satisfying our derived conditions. Furthermore, we analyze how different temperature scaling schemes affect performance in Sec. A.3.

Assigning lower temperatures to FN pairs, pushes the constituent samples far apart. To reduce this effect, we can shift the minimum of the temperature function into the negative half of the cosine similarity vs. temperature plane. The result of this modification can be seen in Table 15. As the contribution corresponding to the FN pairs reduces in  $\frac{\partial \mathcal{L}}{\partial z_i}$  in Eqn. 5, the performance also improves.

## 4 Implementation Details

**Datasets** To study the effects of temperature in the self-supervised contrastive learning framework, we used the ImageNet1K [10] and ImageNet100 [42] datasets. We also used 3 small-scale datasets, namely, CIFAR10 [27] and CIFAR100 [27]. Furthermore, we also study the effect of our proposed framework on the Long-tailed versions of the aforementioned datasets, which we term CIFAR10-LT and CIFAR100-LT (Appendix 5.4).

**Pre-training Details** For the experiments on ImageNet1K and ImageNet100 datasets, we used a ResNet50 [21] backbone for all our experiments. We optimized the network parameters using a LARS optimizer with the square root learning rate scaling scheme as described in the SimCLR [6] paper. For all our experiments we used a batch size of 256, The pre-training and the downstream tasks were run on a single 24GB NVIDIA A5000 GPU using the lightly-ai [41] library. To ensure faster training and prevent out-of-memory issues, we adopted automatic mixed precision (AMP) training. The pre-training details for the CIFAR datasets are provided in the appendix.

**Augmentations** During the pre-training stage, two augmented versions of each input image are generated and used as positive pairs. For the augmentations, we follow the augmentation strategy of SimCLR [6].

## 5 Experimental Results and Ablations

We conducted extensive experiments on the ImageNet100, ImageNet1K, CIFAR10, and CIFAR100 datasets to empirically prove that the proposed temperature scaling framework outperforms the state-of-the-art SSL frameworks and also the recent temperature modulating framework MACL [55]. For pretraining on sentence embeddings, we used the Wiki1M dataset [14].

## 5.1 Comparison with SSL Frameworks on ImageNet100

We consider the vanilla SimCLR as the baseline for our proposed temperature scaling framework, hence all the experiments on ImageNet100 were conducted on the SimCLR framework. We also compare our work with the state-of-the-art contrastive learning frameworks. In Tab. 1, we present results of the vanilla DySTreSS framework and a shifted version of the same (Sec. 5.8) with shift and scale parameters  $\Delta s$  and  $k$ , respectively. The values of  $\tau_{min}$  and  $\tau_{max}$  were set to 0.1 and 0.2, respectively.  $\checkmark$  and  $\times$  in the ‘‘Temp. Scaled’’ column indicates if the corresponding framework uses temperature scaling. SimCLR was used as the baseline in DCL, MACL, and DySTreSS.

**Table 1:** Comparison with state-of-the-art SSL frameworks on ImageNet100 dataset. For DySTreSS\*,  $\Delta s = -0.4, k = 0.7$ . (Here, B. Twins stands for Barlow Twins)

Framework	Temp. Scaled	Lin. Eval. Top-1	Acc. Top-5
SimCLR	$\times$	75.54	93.06
DCL	$\times$	77.38	94.01
BYOL	N/A	75.02	93.42
B. Twins	N/A	75.88	93.96
VicReg	N/A	76.36	94.14
MACL	$\checkmark$	78.28	94.25
DySTreSS	$\checkmark$	78.78	94.70
DySTreSS*	$\checkmark$	<b>78.82</b>	<b>94.76</b>

**Table 2:** Comparison with state-of-the-art SSL frameworks on ImageNet1K dataset (Here, B. Twins stands for Barlow Twins)

Framework	Temp. Scaled	Lin. Eval. Top-1	Acc. Top-5
SimCLR	$\times$	63.2	85.2
DCL	$\times$	65.1	86.2
DCLW	$\times$	64.2	86.0
BYOL	N/A	62.4	82.7
B. Twins	N/A	62.9	84.3
VicReg	N/A	63.0	85.4
MACL	$\checkmark$	64.3	-
DySTreSS	$\checkmark$	<b>65.21</b>	<b>86.55</b>

We observe that the proposed framework outperforms the contemporary state-of-the-art SSL methods on linear probing evaluation. The proposed framework also outperforms the recent state-of-the-art framework MACL [55] which also adopts a temperature-modifying approach on top of the contrastive learning SimCLR framework. Furthermore, we also applied the proposed DySTreSS framework on the SimCLR+DCL framework with the base configuration  $\tau_{min} = 0.1$  and  $\tau_{max} = 0.2$ , and achieved an improvement of 0.14% over the Top-1 accuracy reported in Table 1.

## 5.2 Comparison with SSL Frameworks on ImageNet1K

As the implementation is done using the lightly-ai library, we use the benchmark results provided by the library on the ImageNet1K dataset for the comparison. The results shown in Table 2 are for 100 epochs of pre-training on ImageNet1K. We observe that the proposed framework outperforms the contemporary state-of-the-art self-supervised methods on the ImageNet1K dataset with 100 epochs of pre-training on linear probing accuracy. The results in Table 2 indicate that pre-training with the proposed framework provides better representations that can be easily separable by a linear classifier.

### 5.3 Comparison on Small Scale Benchmarks

In this section, we present the performance of our proposed framework on CIFAR10 and CIFAR100 (Table 3) datasets. We have reported the best results obtained with  $\tau_{min} = 0.07$  and  $\tau_{max} = 0.2$  for comparison in Table 3. From our ablations on CIFAR datasets (Appendix A.3), we observed that the vanilla DySTreSS works better than the shifted versions. On the long-tailed datasets (Table 4 and 5), the DySTreSS outperforms Kukleva et al. [28] after 2000 epochs of pre-training.

**Table 3:** Comparison with SOTA SSL frameworks on CIFAR10 and CIFAR100 datasets.

Framework	Temp. Scaled	CIFAR10	CIFAR100
SimCLR	X	83.65	52.32
MoCoV2	X	83.9	54.01
SimCLR+DCL	X	84.4	56.02
MACL (repro.)	✓	84.85	56.15
DySTreSS	✓	<b>85.68</b>	<b>56.57</b>

**Table 4:** Comparison on long-tailed CIFAR datasets.

Framework	CIFAR10-LT	CIFAR100-LT
Kukleva et al. [28]	62.91	30.20
DySTreSS	<b>64.98</b>	<b>31.71</b>

**Table 5:** Comparison on ImageNet100-LT datasets.

Framework	ImageNet100-LT
Kukleva et al. [28]	45.3 (repro.)
DySTreSS	<b>46.1</b>

On the CIFAR-10 dataset, the proposed framework outperforms the recent state-of-the-art (SOTA) framework MACL [55] along with other contrastive SSL frameworks. On the CIFAR-100 dataset, DySTreSS outperforms SimCLR and MACL by 1.77% and 1.39%, respectively.

### 5.4 Experimental Results on Long-Tailed Datasets

On the long-tailed versions of the CIFAR datasets, the proposed framework improves upon the baseline SimCLR by more than 1%, as seen in tables 6 and 7. ✓ and X in the “Temp. Scaled” column indicates if the corresponding framework uses temperature scaling. We also see in Table 4 and 5, that our proposed method performs better than [28] when pre-trained for 2000 epochs, as per the pre-training configuration in Kukleva et al. [28]. For the experiments on ImageNet100-LT, we used a batch size of 256 for both Kukleva et al. [28] and DySTreSS.

**Table 6:** Comparison with state-of-the-art SSL frameworks on CIFAR10-LT dataset. DySTreSS and DySTreSS\* both have  $\tau_{max} = 0.2$ , but the values of  $\tau_{min}$  are 0.07 and 0.1, respectively.

Framework	Temp. Scaled	Accuracy	
		1-NN	10-NN
SimCLR	X	57.12	55.29
DySTreSS	✓	<b>58.36</b>	56.40
DySTreSS*	✓	58.34	<b>56.54</b>

**Table 7:** Comparison with state-of-the-art SSL frameworks on CIFAR100-LT dataset. DySTreSS and DySTreSS\* both have  $\tau_{max} = 0.2$ , but the values of  $\tau_{min}$  are 0.07 and 0.1, respectively.

Framework	Temp. Scaled	Accuracy	
		1-NN	10-NN
SimCLR	X	28.27	26.18
DySTreSS	✓	<b>29.43</b>	27.10
DySTreSS*	✓	28.82	<b>27.32</b>

## 5.5 Comparison with Negative-free Contrastive and Non-Contrastive Frameworks

For the ImageNet100 dataset, we ran pre-training for 400 epochs with a batch size of 128. We used the same training conditions as in [52] and [51], for a fair comparison. From the results presented in Table 8 and obtained on the ImageNet100 dataset, we can see that our proposed method clearly outperforms the state-of-the-art methods like DINO [5], WMSE [12], Zero-CL [52], and ARB [51]. Linear evaluation task accuracy values for WMSE on the ImageNet100 dataset for 400 epochs pre-training are taken from [52] and [51].

We also present the comparison of the performance of our proposed framework with DINO and WMSE on CIFAR datasets in Table 9. All experiments were done with a batch size of 256 and trained for 200 epochs.

**Table 8:** Comparison of the proposed method with DINO, WMSE, Zero-CL, and ARB on the ImageNet100 dataset on Linear Evaluation task.

Frameworks	Proj. Dim #	Linear Eval. Acc.	
		Top - 1	Top - 5
Barlow Twins [48]	2048	78.62	94.72
VICReg [1]	2048	79.22	95.06
ZeroICL [52]	256	78.02	95.61
ZeroFCL [52]	2048	79.32	94.94
ZeroCL [52]	2048	79.26	94.98
WMSE [12]	256	69.06	91.22
ARB [51]	2048	79.48	95.51
DINO [5]	256	74.84	92.92
BYOL [16]	4096	80.09	94.99
DySTreSS (OURS)	2048	<b>81.24</b>	<b>95.64</b>

**Table 9:** Comparison with DINO and WMSE on CIFAR datasets

Methods	CIFAR10	CIFAR100
DINO	84.02	46.79
WMSE	85.52	52.72
DySTreSS	<b>85.68</b>	<b>56.57</b>

**Table 10:** Comparison of performance on CIFAR datasets for different temperature functions

Function	CIFAR10	CIFAR100
Cosine	85.85	56.57
Linear	85.74	56.78
Exponential	85.81	56.47

## 5.6 Comparison on Transfer Learning Performance

In this section, we compare the proposed framework on two types of transfer learning tasks, each on two different modalities, image and text.

**Transfer Learning on Medical and Natural Image Datasets** In this section, we present the comparison of transfer learning performance on 7 different medical and natural image datasets with different degrees of imbalance. These tasks include both binary and multi-class classification tasks. The encoders were initialized with weights obtained after pre-training for 100 epochs on the ImageNet1K dataset. We also provide the supervised baseline performance as a reference. Implementation details are discussed in detail in Supplementary (Appendix A.2).

From the results presented in Table 11, we can see that the proposed method outperforms SimCLR [6] on all the 7 datasets. The proposed method also outperforms the current state-of-the-art self-supervised contrastive learning algorithm (DCL [47]) on 5 out of 7 datasets. It can also be seen that the

performance of our proposed framework is close to the supervised baseline.

**Table 11:** Performance comparison of the proposed method (DySTreSS) with contemporary self-supervised contrastive state-of-the-art methods on transfer learning tasks. The results of the supervised learning baseline are also provided here for reference.

Datasets	Type	Task	SimCLR [6]	DCL [47]	DySTreSS	Supervised
MURA [38]	Medical	Binary	81.81	81.70	<b>82.27</b>	82.10 [30, 31]
Chaoyang [54]	Medical	Multi-class	83.22	83.12	<b>83.26</b>	83.50 [13]
ISIC2016 [17]	Medical	Binary	85.49	<b>86.02</b>	85.75	85.50 [39]
MHIST [46]	Medical	Binary	83.62	<b>85.26</b>	83.98	86.90 [40]
CIFAR10 [27]	Natural	Multi-class	96.93	97.09	<b>97.14</b>	97.50 [16]
CIFAR100 [27]	Natural	Multi-class	82.99	83.03	<b>83.96</b>	86.40 [16]
Flowers [32]	Natural	Multi-class	93.82	94.11	<b>96.76</b>	97.60 [16]

**Transfer Learning Experiments on Sentence Embedding** Similar to MACL [55], we adopt SimCSE [14] as the baseline for sentence embedding learning. We conduct experiments with BERT [11] on Semantic Textual Similarity (STS) and Transfer tasks following [14]. We can observe from Table 12 that the proposed framework achieves better performance on most STS and transfer tasks over the SimCSE and MACL baseline under the same experimental environment. In support of the difference in reproduced results from the reported results in the respective papers, we speculate the cause to be the difference in the hardware, as already mentioned in [55]. All the experiments were conducted on a 24GB NVIDIA A5500 GPU.

## 5.7 Analysing the Quality of Representations

In this section, we will utilize the following metrics to analyse the quality of representations learnt by some state-of-the-art self-supervised contrastive frameworks on benchmark datasets.

$$\text{Uniformity} = \log \mathbb{E}_{(x_i, x_j) \sim p_{pair}} \exp(-2\|x_i - x_j\|^2) \quad (16)$$

$$\text{Alignment} = \mathbb{E}_{(x_i, x_j) \sim p_{pos}} \|x_i - x_j\|_2^2 \quad (17)$$

where,  $p_{pair}$  and  $p_{pos}$  is joint the distribution of all pairs and positive pairs. Hence, uniformity and alignment behave the same way. A decrease in uniformity value indicates that the distribution of the representations is tending towards a uniform distribution, whereas a decrease in alignment value indicates that the features are being mapped close to each other. Neither can explain the quality of representations by itself. A zero alignment can indicate collapse, while a very negative uniformity value indicates that the representations are not learnt and thus cannot be linearly classified. Hence, a trade-off between alignment and uniformity occurs as explained before. To better understand the quality of representations, researchers often used kNN accuracy or linear classification accuracy on benchmark datasets. We use a metric which is analogous to such metrics, called the inter-class uniformity, which measures the average pair-wise

**Table 12:** Comparison on STS and Transfer tasks (metric: Spearman’s correlation with “all” setting). DySTreSS<sup>+</sup> means DySTreSS with  $\Delta s = -0.2$  and  $k = 0.6$ , DySTreSS\* means DySTreSS with  $\Delta s = -0.4$  and  $k = 0.7$ , DySTreSS\*\* means DySTreSS with  $\Delta s = -0.6$  and  $k = 0.8$

STS Task	STS12	STS13	STS14	STS15	STS16	STSB	SICKR	Avg.
SimCSE (repro.)	65.10	80.32	71.42	80.51	77.80	76.47	70.69	74.62
w/ MACL (repro.)	67.49	81.55	73.21	80.97	77.52	76.54	70.87	74.84
$\tau_{min} = 0.03, \tau_{max} = 0.05$								
w/ DySTreSS	68.00	81.58	73.44	80.33	77.65	76.24	70.98	74.80
w/ DySTreSS <sup>+</sup>	<b>70.19</b>	81.61	73.89	<b>81.91</b>	77.36	77.06	70.01	76.00
w/ DySTreSS*	69.34	81.76	73.51	81.61	77.39	76.67	71.53	75.96
w/ DySTreSS**	69.65	79.18	72.37	80.79	76.83	75.59	71.43	75.12
$\tau_{min} = 0.02, \tau_{max} = 0.05$								
w/ DySTreSS*	69.17	<b>81.69</b>	73.73	81.38	77.75	76.19	70.98	75.84
$\tau_{min} = 0.05, \tau_{max} = 0.07$								
w/ DySTreSS*	69.02	80.61	73.81	81.39	<b>79.75</b>	<b>77.97</b>	<b>72.05</b>	<b>76.37</b>
$\tau_{min} = 0.04, \tau_{max} = 0.05$								
w/ DySTreSS*	69.68	80.33	<b>74.27</b>	80.55	76.89	75.95	70.82	75.50
Transfer Task	MR	CR	SUBJ	MPQA	SST2	TREC	MRPC	Avg.
SimCSE (repro.)	80.42	85.80	94.13	88.66	85.17	87.40	72.29	84.84
w/ MACL (repro.)	80.50	85.41	94.20	89.22	85.06	90.40	<b>75.59</b>	85.77
$\tau_{min} = 0.03, \tau_{max} = 0.05$								
w/ DySTreSS	81.30	87.10	94.79	89.15	86.16	88.20	72.35	85.58
w/ DySTreSS <sup>+</sup>	<b>81.72</b>	86.76	94.34	88.31	86.33	88.00	73.74	85.60
w/ DySTreSS*	81.69	<b>87.28</b>	94.80	89.29	85.83	<b>91.20</b>	72.93	86.15
w/ DySTreSS**	81.62	86.68	94.74	88.75	<b>86.71</b>	90.40	75.30	<b>86.31</b>
$\tau_{min} = 0.02, \tau_{max} = 0.05$								
w/ DySTreSS*	81.59	86.99	94.45	<b>89.48</b>	86.66	87.80	74.90	85.98
$\tau_{min} = 0.05, \tau_{max} = 0.07$								
w/ DySTreSS*	80.69	85.94	94.27	89.16	84.84	89.20	74.61	85.53
$\tau_{min} = 0.04, \tau_{max} = 0.05$								
w/ DySTreSS*	81.02	86.23	<b>94.97</b>	88.86	85.17	89.80	73.22	85.61

distance between the centroids of the clusters. This allows us to understand how much separated are the feature clusters, which is an indicator of how well the semantic representations are learnt.

$$\text{Interclass Uniformity} = \log \mathbb{E}_{(x_i, x_j) \sim p_{centroids}} \exp(-2\|x_i - x_j\|^2) \quad (18)$$

where,  $p_{centroids}$  denote the joint distribution of class centroids. A high Interclass Uniformity means that the clusters of the classes are close to each other. Hence, the lower the better.

In Table 13, we provide the overall uniformity and inter-class uniformity of SimCLR, MoCov2, DCL, and DCLW along with our proposed framework. These values are obtained after pretraining on CIFAR10, CIFAR100, and ImageNet1K datasets. Please note that the reported values are for pre-training of 200 epochs, 200 epochs, and 100 epochs for CIFAR10, CIFAR100, and ImageNet1K datasets, respectively. For other epoch numbers, these values are subject to change as the feature representations evolve depending on the convergence of the algorithm.

A lower uniformity value indicates that the samples are more spread out than a model with a higher uniformity value. The inter-class uniformity metric value



**Table 13:** Uniformity, Alignment, Inter-Class Uniformity metric values for CIFAR10, CIFAR100 and ImageNet1K datasets.

Method	Uniformity	Alignment	Inter-Class Uniformity	Accuracy
CIFAR10				
SimCLR	-2.2135	1.5784	-0.5194	83.65
MoCov2	-2.1929	1.47393	-0.5094	83.67
DCLW	-2.5482	1.5632	-0.5349	84.02
DCL	-2.7717	1.6181	-0.5524	84.47
DySTreSS	-2.8430	1.6310	-0.5797	85.83
CIFAR100				
SimCLR	-2.2556	1.4661	-0.5246	52.32
MoCov2	-2.2202	1.4444	-0.5364	54.01
DCLW	-2.6865	1.5425	-0.6405	55.87
DCL	-2.8314	1.5723	-0.6792	56.02
DySTreSS	-2.8169	1.5408	-0.7657	56.72
ImageNet1K				
SimCLR	-2.9084	1.5253	-0.8739	63.2
DCLW	-3.0137	1.5295	-0.9544	64.2
DCL	-3.0786	1.5335	-1.0053	65.1
DySTreSS	-3.0596	1.5278	-1.0015	65.2

indicates how far apart the class centroids are from one another. Hence, a lower inter-class uniformity value indicates that the clusters are more separated than a mode with a higher value. We see that the overall uniformity values are the lowest for our proposed method. In fact, we can see a trend in the uniformity values with the accuracy for different models as well. In our case, the inter-class uniformity metric is the lowest, which means that the class centroids are farther away than the other models, and is an indicator of how easily separable the clusters are for our proposed method. Thus, we can say that the proposed framework improves feature representations, and hence, learns more separable clusters, resulting in higher 200-NN accuracy.

## 5.8 Ablation Studies

**Ablation on Different Temperature Functions** In this section, we present the performance of different temperature functions, namely linear and exponential on CIFAR datasets. From Table 10, we see that all the temperature functions perform similarly to the cosine function, if not better. All the temperature functions satisfy the conditions of positive and negative slopes on the positive and negative half of the temperature vs. cosine similarity plane, respectively. All experiments were run for 200 epochs, and the results reported are for 200-NN Top-1 accuracy.

**Effect of Temperature Range** To find the optimal range of temperature, we conduct pre-training with several temperature ranges on the ImageNet100 dataset as given in Table 14 and find that the values  $\tau_{min} = 0.1$  and  $\tau_{max} = 0.2$  gives the best performance. The temperature functions for different temperature ranges are also shown in Figure 3. We observe that setting the value of  $\tau_{max}$  towards high degrades performance, whereas setting both  $\tau_{max}$  and  $\tau_{min}$  towards low also degrades performance. The reason for such behavior can be understood from the uniformity and tolerance plots in Fig. 5. For the settings given in Tab. 14, the interclass uniformity (See Eqn. 18, App. Sec. ??) are -0.6584, -0.7202, -0.7422, -0.7710, respectively. As theorized, for the worst-performing case, we can see that due to low temperature, the tolerance is high but the interclass uniformity is high too, deviating from the ideal global structure (Sec. 3.3). Whereas for the second worst-performing case, we can see that due to the high temperature, the global structure is again disrupted as an increase in uniformity means the samples are more spread out, gain in accuracy is solely due to a decrease in interclass uniformity. In the rest of the cases, tolerance is high and the interclass uniformity is also low, indicating that the interclass distance is high, facilitating better classification.

**Table 14:** Ablation of DySTreSS on different temperature ranges on ImageNet100 dataset.

$\tau_{min}$	$\tau_{max}$	20NN Acc.		Lin. Eval. Acc.	
		Top-1	Top-5	Top-1	Top-5
0.07	0.1	67.18	87.82	77.28	94.16
0.07	0.5	67.88	88.22	76.34	93.72
0.07	0.2	71.46	89.42	78.46	94.4
0.1	0.2	72.00	89.76	78.76	94.7

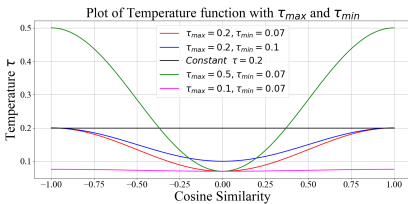


**Fig. 3:** Temperature functions for different  $\tau_{max}$  and  $\tau_{min}$ . Best visible at 200%.

**Table 15:** Ablation on different temperature profiles on ImageNet100 dataset.

shift	scale	20-NN Accuracy		Lin. Eval. Acc.	
		Top-1	Top-5	Top-1	Top-5
0.0	0.5	71.66	90.16	78.46	94.86
0.2	0.6	71.58	89.14	78.56	94.38
0.4	0.7	71.58	89.58	78.46	94.54
-0.2	0.6	72.38	89.99	78.78	94.59
-0.4	0.7	71.58	90.16	78.82	94.76

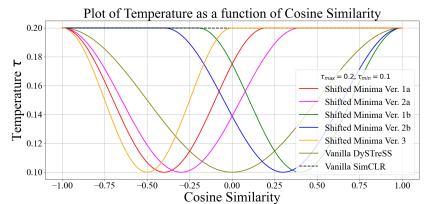


**Fig. 4:** Plot of shifted versions of Temperature functions. Best visible at 200%.

**Effect of Shifted Temperature Profiles** Similar to the previous ablation study, we look to find the optimal temperature profile over the cosine similarity spectrum by shifting the minima of the temperature profile to the left or right as depicted in Figure 4. When applying a shift ( $\Delta s$ ) to the minima at  $s = 0.0$ , we also scale the temperature profile by  $k$  to ensure that the temperatures at the extremities of the cosine similarity spectrum ( $s = \pm 1.0$ ) remain at  $\tau_{max}$  according to our assumptions in Sec. 3.3. The algorithm for computing the values of the shifted temperature functions is presented in Algorithm 2.

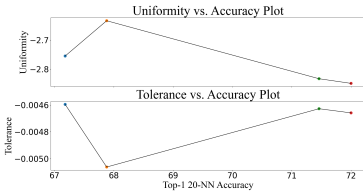


**Fig. 5:** Plot of Uniformity and Tolerance vs. 20NN Top-1 acc. shown in Table 14. Best visible at 300%.

We primarily use three different shifted versions of the temperature profile for the ablations on the ImageNet100 dataset. In the first version, Shifted Minima Ver. 1, we shift the minima towards the right half-plane. In the second version, Shifted Minima Ver. 2, we shift the minima towards the left half plane. In the last and third versions, we shift the temperature profile entirely in the left half plane and keep the temperature constant in the right half plane. In addition to the shift, we apply appropriate scaling such that the extremities have maximum temperature. The algorithm for calculating the temperature for the shifted temperature profile is given in Algorithm 2. We observe from the results presented in Table 15, that a shift of  $\Delta s = -0.4$  from  $s = 0.0$  and a scaling of  $k = 0.7$  yields the best linear evaluation performance on the ImageNet100 dataset.

---

**Algorithm 2:** Shifted Temperature Functions

---

```

Data:  $\tau_{max}, \tau_{min}, \Delta\tau = \tau_{max} - \tau_{min}, \Delta s, k$ 
Input:  $s_{ij} \rightarrow$  Cosine Similarity of  $(x_i, x_j)$ 
if  $(\Delta s \leq 0 \wedge s_{ij} \leq -\Delta s) \vee (\Delta s \geq 0 \wedge s_{ij} \geq -\Delta s)$ 
  then
     $\tau_{ij} = \tau_{min} + \frac{\Delta\tau}{2} (1 + \cos(\frac{\pi}{k} (\Delta s + s_{ij})))$ 
  else
     $\tau_{ij} = \tau_{max}$ 

```

---

## 6 Conclusion

In this work, we identified a specific category of pairs in self-supervised contrastive learning and analyzed the effect of temperature on such pairs in optimizing InfoNCE loss. We observed that by varying the temperature as a function of the cosine similarity values of the feature vectors of all pairs, we can control the dynamics of the optimization process and improve the performance of the baseline method, SimCLR. Through extensive experiments, we show that the proposed framework improves performance over the baseline and state-of-the-art algorithms. Finally, this work lays the foundation for further research into the working principle and dynamics of the InfoNCE loss function.

## References

1. Bardes, A., Ponce, J., LeCun, Y.: Vicreg: Variance-invariance-covariance regularization for self-supervised learning. In: The Tenth International Conference on Learning Representations, ICLR 2022, Virtual Event, April 25-29, 2022. OpenReview.net (2022), <https://openreview.net/forum?id=xm6YD62D1Ub> 3, 14
2. Bautista, M.A., Sanakoyeu, A., Tikhoncheva, E., Ommer, B.: Cliquecnn: Deep unsupervised exemplar learning. In: NeurIPS (2016) 3
3. Caron, M., Bojanowski, P., Joulin, A., Douze, M.: Deep clustering for unsupervised learning of visual features. In: ECCV (2018) 3

4. Caron, M., Misra, I., Mairal, J., Goyal, P., Bojanowski, P., Joulin, A.: Unsupervised learning of visual features by contrasting cluster assignments. In: *NeurIPS (2020)* **3**
5. Caron, M., Touvron, H., Misra, I., Jégou, H., Mairal, J., Bojanowski, P., Joulin, A.: Emerging properties in self-supervised vision transformers. In: *2021 IEEE/CVF International Conference on Computer Vision, ICCV 2021, Montreal, QC, Canada, October 10-17, 2021*. pp. 9630–9640. IEEE (2021). <https://doi.org/10.1109/ICCV48922.2021.00951>, <https://doi.org/10.1109/ICCV48922.2021.00951> **3, 14**
6. Chen, T., Kornblith, S., Norouzi, M., Hinton, G.E.: A simple framework for contrastive learning of visual representations. In: *ICML (2020)* **1, 2, 3, 4, 10, 11, 14, 15, 24**
7. Chen, T., Kornblith, S., Swersky, K., Norouzi, M., Hinton, G.E.: Big self-supervised models are strong semi-supervised learners. In: *NeurIPS (2020)* **3**
8. Chen, X., Fan, H., Girshick, R.B., He, K.: Improved baselines with momentum contrastive learning. *CoRR* **abs/2003.04297** (2020), <https://arxiv.org/abs/2003.04297> **3, 24**
9. Chen, X., He, K.: Exploring simple siamese representation learning. In: *CVPR (2021)* **3**
10. Deng, J., Dong, W., Socher, R., Li, L.J., Li, K., Fei-Fei, L.: Imagenet: A large-scale hierarchical image database. In: *CVPR (2009)* **11, 24**
11. Devlin, J., Chang, M.W., Lee, K., Toutanova, K.: Bert: Pre-training of deep bidirectional transformers for language understanding. In: *North American Chapter of the Association for Computational Linguistics (2019)*, <https://api.semanticscholar.org/CorpusID:52967399> **15**
12. Ermolov, A., Siarohin, A., Sangineto, E., Sebe, N.: Whitening for self-supervised representation learning. In: Meila, M., Zhang, T. (eds.) *Proceedings of the 38th International Conference on Machine Learning, ICML 2021, 18-24 July 2021, Virtual Event. Proceedings of Machine Learning Research*, vol. 139, pp. 3015–3024. PMLR (2021), <http://proceedings.mlr.press/v139/ermolov21a.html> **3, 14**
13. Galdran, A., Verjans, J.W., Carneiro, G., González Ballester, M.A.: Multi-head multi-loss model collaboration. In: Greenspan, H., Madabhushi, A., Mousavi, P., Salcudean, S., Duncan, J., Syeda-Mahmood, T., Taylor, R. (eds.) *Medical Image Computing and Computer Assisted Intervention – MICCAI 2023*. pp. 108–117. Springer Nature Switzerland, Cham (2023) **15**
14. Gao, T., Yao, X., Chen, D.: SimCSE: Simple contrastive learning of sentence embeddings. In: *Proceedings of the 2021 Conference on Empirical Methods in Natural Language Processing*. pp. 6894–6910. Association for Computational Linguistics, Online and Punta Cana, Dominican Republic (Nov 2021). <https://doi.org/10.18653/v1/2021.emnlp-main.552>, <https://aclanthology.org/2021.emnlp-main.552> **11, 15**
15. Goodfellow, I., Pouget-Abadie, J., Mirza, M., Xu, B., Warde-Farley, D., Ozair, S., Courville, A., Bengio, Y.: Generative adversarial networks (2014) **3**
16. Grill, J.B., Strub, F., Altché, F., Tallec, C., et al.: Bootstrap your own latent - a new approach to self-supervised learning. In: *NeurIPS (2020)* **3, 14, 15**
17. Gutman, D., Codella, N.C.F., Celebi, E., Helba, B., Marchetti, M., Mishra, N., Halpern, A.: Skin lesion analysis toward melanoma detection: A challenge at the international symposium on biomedical imaging (isbi) 2016, hosted by the international skin imaging collaboration (isic). *CoRR* **abs/1605.01397** (2016), <https://arxiv.org/abs/1605.01397> **15**
18. Gutmann, M., Hyvärinen, A.: Noise-contrastive estimation: A new estimation principle for unnormalized statistical models. In: *AISTATS (2010)* **3**
19. He, K., Fan, H., Wu, Y., Xie, S., Girshick, R.B.: Momentum contrast for unsupervised visual representation learning. In: *CVPR (2020)* **1, 2, 3, 4**

20. He, K., Zhang, X., Ren, S., Sun, J.: Delving deep into rectifiers: Surpassing human-level performance on imagenet classification. In: ICCV (2015) [24](#)
21. He, K., Zhang, X., Ren, S., Sun, J.: Deep residual learning for image recognition. In: CVPR (2016) [11](#), [24](#)
22. Huang, J., Dong, Q., Gong, S., Zhu, X.: Unsupervised deep learning by neighbourhood discovery. In: ICML (2019) [3](#)
23. Ioffe, S., Szegedy, C.: Batch normalization: Accelerating deep network training by reducing internal covariate shift. In: ICML (2015) [24](#)
24. Jing, L., Tian, Y.: Self-supervised visual feature learning with deep neural networks: A survey. IEEE TPAMI (2020) [3](#)
25. Khosla, P., Teterwak, P., Wang, C., Sarna, A., Tian, Y., Isola, P., Maschinot, A., Liu, C., Krishnan, D.: Supervised contrastive learning. In: NeurIPS (2020) [6](#)
26. Kingma, D.P., Welling, M.: Auto-encoding variational bayes. arXiv preprint arXiv:1312.6114 (2013) [3](#)
27. Krizhevsky, A.: Learning multiple layers of features from tiny images (2009), <https://www.cs.toronto.edu/~kriz/learning-features-2009-TR.pdf> [11](#), [15](#)
28. Kukleva, A., Böhle, M., Schiele, B., Kuehne, H., Rupperecht, C.: Temperature schedules for self-supervised contrastive methods on long-tail data. In: The Eleventh International Conference on Learning Representations (2023), <https://openreview.net/forum?id=ejHUr4nfHhD> [2](#), [3](#), [13](#), [24](#)
29. Ledig, C., Theis, L., Huszár, F., Caballero, J., et al.: Photo-realistic single image super-resolution using a generative adversarial network. In: CVPR (2017) [3](#)
30. Nauta, M., Hegeman, J.H., Geerdink, J., Schlötterer, J., van Keulen, M., Seifert, C.: Interpreting and correcting medical image classification with pip-net (2023) [15](#)
31. Nauta, M., Schlötterer, J., van Keulen, M., Seifert, C.: Pip-net: Patch-based intuitive prototypes for interpretable image classification. In: Proceedings of the IEEE/CVF Conference on Computer Vision and Pattern Recognition (CVPR). pp. 2744–2753 (June 2023) [15](#)
32. Nilsback, M.E., Zisserman, A.: A visual vocabulary for flower classification. In: IEEE Conference on Computer Vision and Pattern Recognition. vol. 2, pp. 1447–1454 (2006) [15](#)
33. Noroozi, M., Favaro, P.: Unsupervised learning of visual representations by solving jigsaw puzzles. In: ECCV (2016) [1](#)
34. Oord, A.v.d., Li, Y., Vinyals, O.: Representation learning with contrastive predictive coding. arXiv preprint arXiv:1807.03748 (2018) [2](#), [4](#)
35. Pathak, D., Krahenbuhl, P., Donahue, J., Darrell, T., Efros, A.A.: Context encoders: Feature learning by inpainting. In: CVPR (2016) [1](#)
36. Pathak, D., Krahenbuhl, P., Donahue, J., Darrell, T., Efros, A.A.: Context encoders: Feature learning by inpainting. In: CVPR (2016) [3](#)
37. Qiu, Z., Hu, Q., Yuan, Z., Zhou, D., Zhang, L., Yang, T.: Not all semantics are created equal: Contrastive self-supervised learning with automatic temperature individualization. In: Krause, A., Brunskill, E., Cho, K., Engelhardt, B., Sabato, S., Scarlett, J. (eds.) International Conference on Machine Learning, ICML 2023, 23-29 July 2023, Honolulu, Hawaii, USA. Proceedings of Machine Learning Research, vol. 202, pp. 28389–28421. PMLR (2023), <https://proceedings.mlr.press/v202/qiu23a.html> [4](#)
38. Rajpurkar, P., Irvin, J., Bagul, A., Ding, D.Y., Duan, T., Mehta, H., Yang, B., Zhu, K., Laird, D., Ball, R.L., Langlotz, C.P., Shpanskaya, K.S., Lungren, M.P., Ng, A.Y.: MURA dataset: Towards radiologist-level abnormality detection in musculoskeletal radiographs. CoRR [abs/1712.06957](https://arxiv.org/abs/1712.06957) (2017), <http://arxiv.org/abs/1712.06957> [15](#)

39. for Digital Imaging of the Skin (ISDIS), I.S.: <https://challenge.isic-archive.com/leaderboards/2016/>, <https://challenge.isic-archive.com/leaderboards/2016/15>
40. Springenberg, M., Frommholz, A., Wenzel, M., Weicken, E., Ma, J., Strothoff, N.: From modern cnns to vision transformers: Assessing the performance, robustness, and classification strategies of deep learning models in histopathology. *Medical Image Analysis* **87**, 102809 (2023). <https://doi.org/https://doi.org/10.1016/j.media.2023.102809>, <https://www.sciencedirect.com/science/article/pii/S1361841523000701> 15
41. Susmelj, I., Helle, M., Wirth, P., Prescott, J., et al., M.E.: *Lightly* (2020) 11
42. Tian, Y., Krishnan, D., Isola, P.: Contrastive multiview coding. In: Vedaldi, A., Bischof, H., Brox, T., Frahm, J.M. (eds.) *ECCV* (2020) 11
43. Wang, F., Liu, H.: Understanding the behaviour of contrastive loss. In: *CVPR* (2021) 2, 3, 4, 6
44. Wang, F., Liu, H.: Understanding the behaviour of contrastive loss. In: *CVPR* (2021) 28
45. Wang, T., Isola, P.: Understanding contrastive representation learning through alignment and uniformity on the hypersphere. In: *ICML* (2020) 6
46. Wei, J.W., Suriawinata, A.A., Ren, B., Liu, X., Lisovsky, M., Vaickus, L.J., Brown, C., Baker, M., Tomita, N., Torresani, L., Wei, J., Hassanpour, S.: A petri dish for histopathology image analysis. In: Tucker, A., Abreu, P.H., Cardoso, J.S., Rodrigues, P.P., Riaño, D. (eds.) *Artificial Intelligence in Medicine - 19th International Conference on Artificial Intelligence in Medicine, AIME 2021, Virtual Event, June 15-18, 2021, Proceedings. Lecture Notes in Computer Science*, vol. 12721, pp. 11–24. Springer (2021). [https://doi.org/10.1007/978-3-030-77211-6\\_2](https://doi.org/10.1007/978-3-030-77211-6_2), [https://doi.org/10.1007/978-3-030-77211-6\\_2](https://doi.org/10.1007/978-3-030-77211-6_2) 15
47. Yeh, C.H., Hong, C.Y., Hsu, Y.C., Liu, T.L., Chen, Y., LeCun, Y.: Decoupled contrastive learning. In: *Computer Vision – ECCV 2022*. pp. 668–684. Springer Nature Switzerland, Cham (2022) 1, 3, 14, 15
48. Zbontar, J., Jing, L., Misra, I., LeCun, Y., Deny, S.: Barlow twins: Self-supervised learning via redundancy reduction. In: *International Conference on Machine Learning*. pp. 12310–12320. PMLR (2021) 3, 14
49. Zhang, O., Wu, M., Bayrooti, J., Goodman, N.D.: Temperature as uncertainty in contrastive learning. *arXiv abs/2110.04403* (2021), <https://arxiv.org/abs/2110.04403> 3
50. Zhang, R., Isola, P., Efros, A.A.: Colorful image colorization. In: *ECCV* (2016) 1, 3
51. Zhang, S., Qiu, L., Zhu, F., Yan, J., Zhang, H., Zhao, R., Li, H., Yang, X.: Align representations with base: A new approach to self-supervised learning. In: *IEEE/CVF Conference on Computer Vision and Pattern Recognition, CVPR 2022, New Orleans, LA, USA, June 18-24, 2022*. pp. 16579–16588. IEEE (2022). <https://doi.org/10.1109/CVPR52688.2022.01610>, <https://doi.org/10.1109/CVPR52688.2022.01610> 3, 14
52. Zhang, S., Zhu, F., Yan, J., Zhao, R., Yang, X.: Zero-cl: Instance and feature decorrelation for negative-free symmetric contrastive learning. In: *The Tenth International Conference on Learning Representations, ICLR 2022, Virtual Event, April 25-29, 2022*. OpenReview.net (2022), <https://openreview.net/forum?id=RAW9tCdVxLj> 3, 14
53. Zhou, J., Wei, C., Wang, H., Shen, W., Xie, C., Yuille, A., Kong, T.: ibot: Image bert pre-training with online tokenizer. *International Conference on Learning Representations (ICLR)* (2022) 3

54. Zhu, C., Chen, W., Peng, T., Wang, Y., Jin, M.: Hard sample aware noise robust learning for histopathology image classification. *IEEE Trans. Medical Imaging* **41**(4), 881–894 (2022). <https://doi.org/10.1109/TMI.2021.3125459>, <https://doi.org/10.1109/TMI.2021.3125459> 15
55. Zizheng, H., Haoxing, C., Ziqi, W., Chao, Z., Huaxiong, L., Bo, W., Chunlin, C.: Model-aware contrastive learning: Towards escaping the dilemmas. In: *ICML* (2023) 3, 11, 12, 13, 15

## A Small Scale Benchmarks

### A.1 Pre-Training Implementation Details

The encoder used in the pre-training model for experiments on CIFAR10 and CIFAR100 is ResNet18 [21]. The first convolutional layer in ResNet18 is replaced by a convolutional layer with a kernel of dimension  $3 \times 3$  and the subsequent Max-pooling layer is removed. Similarly, for CIFAR10-LT and CIFAR100-LT, we used the aforementioned ResNet18, as well. However, for the experiments on Tiny-ImageNet, we use the original ResNet50 [21]. The last fully connected layer from the ResNet network is removed for all experiments, and the output obtained from the ResNet encoder is fed into a 2-layer multi-layered perceptron (MLP) network called Projector. For the projector architecture, we follow the SimCLR [6], where the Linear layers are followed by Batch Normalization (BN) [23] layers, with a ReLU [20] activation function in between the first BN layer and the second Linear layer. For the pre-training procedure, we use SGD optimizer (momentum= 0.9, weight decay factor=  $5e - 4$ ) with a learning rate of 0.06 and batch size of 128 for all datasets. For the balanced CIFAR and Tiny-ImageNet datasets, we run the optimization procedure for 200 epochs. For the long-tailed versions of the CIFAR datasets, we adopted 500 epochs of training [28].

For the evaluation stage, we adopt a kNN classifier. For the balanced CIFAR and Tiny-ImageNet datasets, we used a kNN classifier with  $k = 200$ , with weights based on cosine similarity. For long-tailed versions of the CIFAR datasets, we used a  $k$  value of 1 and 10 with weights based on distance  $L2$ . All the training and inference were run on a 16GB NVIDIA P100 GPU. Since the proposed framework is based on InfoNCE, the computation overhead is the same as contemporary frameworks such as SimCLR [6], MoCov2 [8], etc.

### A.2 Transfer Learning Implementation Details

We fine-tuned the models pre-trained on the ImageNet1K [10] dataset for 50 epochs using an SGD optimizer. We used class weights to mitigate the effect of imbalance in all datasets, except the natural image datasets. For the MURA, ISIC2016, and MHIST datasets, we used positive class weights of 0.7097, 4.24, and 2.45, respectively. For the Chaoyang dataset, the class weights used were 1.264, 1.667, 1.0, and 2.114 for the 4 classes. For all the experiments, a batch size of 128 was used. For the multiclass and binary classification tasks, we used a learning rate of 0.1 and 1.0, respectively, and a multistep decay scheduler with a decay by a factor of 0.1 at the 30th and 40th epochs.

### A.3 Ablation Studies on CIFAR datasets

**Effect of Different Temperature Ranges on CIFAR datasets** The performance of the proposed framework also varies as the values of  $\tau_{max}$  and  $\tau_{min}$  are varied. We experimented with different temperature ranges as given in Fig. 3 and observed that the proposed framework achieves the best accuracy in the



temperature range  $\tau_{min} = 0.07$  to  $\tau_{max} = 0.2$  for both the CIFAR datasets. The different temperature range affects different types of samples differently. It is evident from Fig. 6, an increase in temperature causes a decrease in uniformity. For example, for temperature ranges  $((\tau_{min}, \tau_{max}), (0.2, 0.5)$  and  $(0.2, 0.2)$ , we see a decrease in uniformity and an increase in tolerance. Whereas, for temperature ranges with lower  $\tau_{min}$  but the same  $\tau_{max}$ , the general trend shows that the uniformity is greater and tolerance is lower. This conforms with our theory in Sec. 3.3. On the contrary, for CIFAR100, due to the presence of *more true negative pairs* than CIFAR10, increasing temperature inhibits the uniformity (tolerance) from increasing (decreasing) sufficiently to improve performance. Hence, for the same  $\tau_{min}$ , the performance was better for a lower  $\tau_{max}$ .

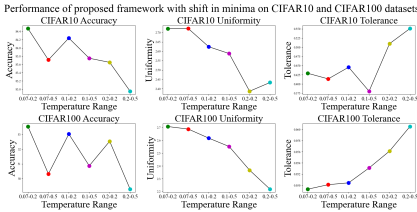


**Fig. 6:** Plot of Accuracy on CIFAR10 (top) and CIFAR100 (bottom) datasets for different temperature ranges. The figure is best visible at 500%.

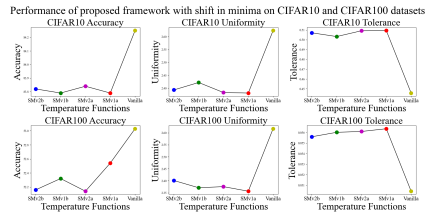


**Fig. 7:** Plot of Accuracy, Uniformity, and Tolerance with a shift in minima for CIFAR10 (top) and CIFAR100 (bottom) dataset. The colour codes are matched to the curves in Fig. 4. The figure is best visible at 500%.

**Effect of Shifted Temperature Profiles on CIFAR datasets** In Fig. 7, we present the accuracy, uniformity, and tolerance values for different temperature functions given in Fig. 4. We observe that shifting the minimum of the temperature function influences different samples and consequently changes the structure of the feature space and performance accordingly. Along the x-axis in Fig. 7, ‘SMvx’ denotes ‘Shifted Minima Version x’. ‘Ver. xa’ and ‘Ver. xb’ denotes two shifts of  $-0.2$  and  $-0.4$  from the origin. For the CIFAR10 dataset, we can observe that a shift of  $-0.2$  is better than a shift of  $-0.4$ , while the reverse is true for the CIFAR100 dataset. However, none of the configurations yields better results than the vanilla version with no shift. A lower temperature towards  $s_{ij} = -1$  increases uniformity, as evident from the difference in uniformity between SMv1b and SMv2b or SMV1a and SMv2a, while the reverse is true for tolerance. The drop in performance is primarily due to the fact that a constant temperature in the range  $[-\tau_{shift}, 1.0] \mid (\tau_{shift} \in \{-0.2, -0.4\})$  caused by the shift results in decreased repulsion of the hard true negative samples, delaying convergence.

**Effect of Learning Rate** As the temperature is decreased, the displacement gradients (Eqn. 5) increase, resulting in an increase in the magnitude of fluctuations from false negative pairs. A low learning rate plays a crucial role in this scenario in smoothening out the fluctuations. On the contrary, at a high learning rate, the fluctuations are amplified and should degrade the performance. However, from Fig. 8, we observe this effect for CIFAR10 only, as the number of false negative pairs in a batch is greater than that in CIFAR100.

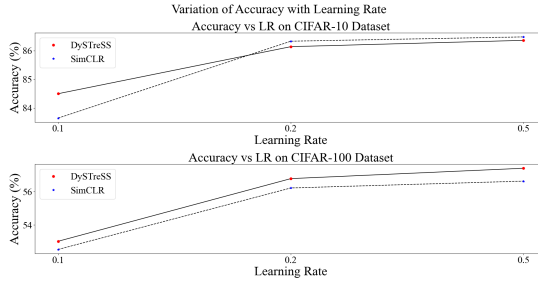


**Fig. 8:** Plot of Accuracy with change in Learning Rate for the datasets CIFAR10 (top) and CIFAR100 (bottom). The figure is best visible at 500%.

## B Pseudocode for Vanilla DySTreSS

---

### Algorithm 3: PyTorch-style pseudocode for Vanilla DySTreSS

---

```

# f: Encoder Network, N: Batch Size, XEnt: Cross Entropy Loss
# tmin, tmax: Minimum Temperature, Maximum Temperature
for x in loader:
    # Augment to generate positive pairs
    x_1, x_2 = augment(x)
    # Pass through the encoder to get feature vectors
    z_1, z_2 = f(x_1), f(x_2)
    # L2-Normalize the feature vectors
    z_1, z_2 = F.normalize(z_1, dim=-1), F.normalize(z_2, dim=-1)
    # Generate Cosine Similarity matrix
    s11 = z_1 @ z_1.T
    s22 = z_2 @ z_2.T
    s12 = z_1 @ z_2.T
    s21 = z_2 @ z_1.T
    # Generate Similarity matrix mask
    dg, ndg = torch.eye(N), 1 - torch.eye(N)
    # Segregate the positive pair cosine similarity values
    s11, s22 = s11[ndg].view(N,-1), s22[ndg].view(N,-1)
    # Segregate the negative pair cosine similarity values
    s1211 = torch.cat([s12, s11], dim=1)
    s2122 = torch.cat([s21, s22], dim=1)
    s = torch.cat([s1211, s2122], dim=0)
    temp = tmin + 0.5(tmax - tmin)(1 + cos(π(1 + s.detach())))
    s = s / temp
    labels = torch.arange(N).repeat(2)
    # Compute Cross Entropy loss
    loss = XEnt(logits, labels)
    # Optimize Loss
    loss.backward()
    optimizer.step()

```

---

## C Do we really need high temperature in low cosine similarity region?

In this section, we explore if we need the temperature values to be high in the low cosine similarity region. We experimented with monotonous cosine functions with minimum at  $s_{ij} = -1$  and maximum at  $s_{ij} = +1$  on the CIFAR datasets. We observed, that using a monotonous cosine function did not degrade performance on the benchmark datasets. From the observed results in Table 16, we can infer that the distribution of false negative samples does not extend towards  $s_{ij} = -1$ .

Also, we can say that, a low temperature on the true negative pairs with cosine similarity in the neighborhood of  $s_{ij} = -1$ , does not contribute much to the representation learning. This conclusion agrees with the findings of [44]. Hence, we do not see any major effect on the performance.

Like easy negative samples, we also consider the possibility of samples that form hard false negative pairs (samples in negative pairs belonging to the same ground truth classes). In the pre-training stage, we can't have access to the ground truth labels, hence cannot say for certain the range of cosine similarities for false negative pairs in the pre-training stage where the weights are initialized randomly. Also, we wouldn't want the samples to drift farther away from each other and hence, we keep a higher temperature towards low cosine similarity.

**Table 16:** Comparison of performance on CIFAR datasets for monotonous temperature functions.

Function	CIFAR10	CIFAR100
Proposed Cosine	85.85	56.57
Monotonic Cosine	85.84	56.21